ANL/FPP/TM--244

DE90 004422

Distribution Category:
Plasma Fusion Systems
(UC-421)
Theoretical Plasma Physics
(UC-427)

ANL/FPP/TM-244

ARGONNE NATIONAL LABORATORY
9700 South Cass Avenue
Argonne, Illinois 60439-4801

NEAR-SURFACE SPUTTERED PARTICLE TRANSPORT FOR AN OBLIQUE INCIDENCE MAGNETIC FIELD PLASMA

Jeffrey N. Brooks
Fusion Power Program
Engineering Physics Division

November 1989

Work supported by

Office of Fusion Energy
U.S. Department of Energy
Under Contract W-31-109-Eng-38

TABLE OF CONTENTS

LIST OF FIGURES

LIST OF TABLES

NEAR-SURFACE SPUTTERED PARTICLE TRANSPORT FOR AN OBLIQUE INCIDENCE MAGNETIC FIELD PLASMA

J.N. Brooks
Argonne National Laboratory

ABSTRACT

Near-surface sputtered particle transport has been analyzed numerically using models of sputtering, sheath parameters, and impurity collisions with a background D-T plasma. Tungsten and carbon sputtering was examined, for tokamak divertor plasma conditions. Redeposited ion parameters computed include the charge state, transit time, energy and angle of incidence. A regime of operation for finite self-sputtering of tungsten has been identified. This regime is broader than previous estimates. Results for energetically sputtered and thermally sputtered carbon are compared.

1. INTRODUCTION

Surface erosion by sputtering in tokamaks depends heavily on the transport of sputtered and subsequently redeposited surface atoms [1]. Data on redeposited charge states, energy, etc. is needed for input to codes such as REDEP [1] in order to make estimates of surface erosion. Data is also needed to assess the effect of sputtered impurities on the local plasma. An early analysis of this subject [2] used a sheath model appropriate to a normal incidence magnetic field, and used a simplified treatment of plasma-impurity ion collisions. More information is now known about the probable structure of the plasma sheath for oblique incidence magnetic field geometry [3-6]. Such geometry applies to most present and proposed impurity control surfaces in tokamaks, namely poloidal divertors and toroidal limiters. The sheath structure is particularly important to sputtered particle transport for the high plasma densities associated with high recycle divertors.

To analyze the sputtered particle transport, a Monte Carlo code, WBC was developed, based on models of sputtering, plasma sheath parameters, and collisions of the sputtered particles with a fixed background D-T plasma. The code computes the sputtered neutral transport and ionization, and the sub-gyro orbit motion of the resulting impurity ions. The ion motion is computed by solving for the Lorentz force motion, charge changing collisions with the electrons, and velocity changing collisions with the DT ions and electrons.

Transport of sputtered tungsten and carbon was examined. It is found that redeposited tungsten ions acquire lower charge states and energies, and have lower self-sputtering coefficients than previous estimates. This is due to the much larger width of the oblique incidence sheath. Physically sputtered carbon is also affected, although to a lesser extent, by the sheath structure. Low energy sputtered carbon (from radiation enhanced sublimation) is found to acquire a smaller but still significant energy, than physically sputtered material.

The role of several phenomena associated with a high-recycle divertor has also been examined. These are viscosity effects, thermal forces, and radial electric fields. It is found that only the latter has a significant effect on near-surface sputtered particle transport.

2. MODEL

2.1 Neutral Transport

Figure 1 shows the model geometry. The magnetic field lies in the z-y plane and is uniform in the x-direction. The plasma is uniform in the x-y plane. Surface atoms are sputtered with a velocity determined from the following probability density function:

$$f(E,\theta,\phi) = f_1(E)\, f_2(\theta)\, f_3(\phi) \qquad (1)$$

for energy E and elevation and azimuth angles θ and ϕ. For tungsten and physically sputtered carbon, the energy distribution is given by the random

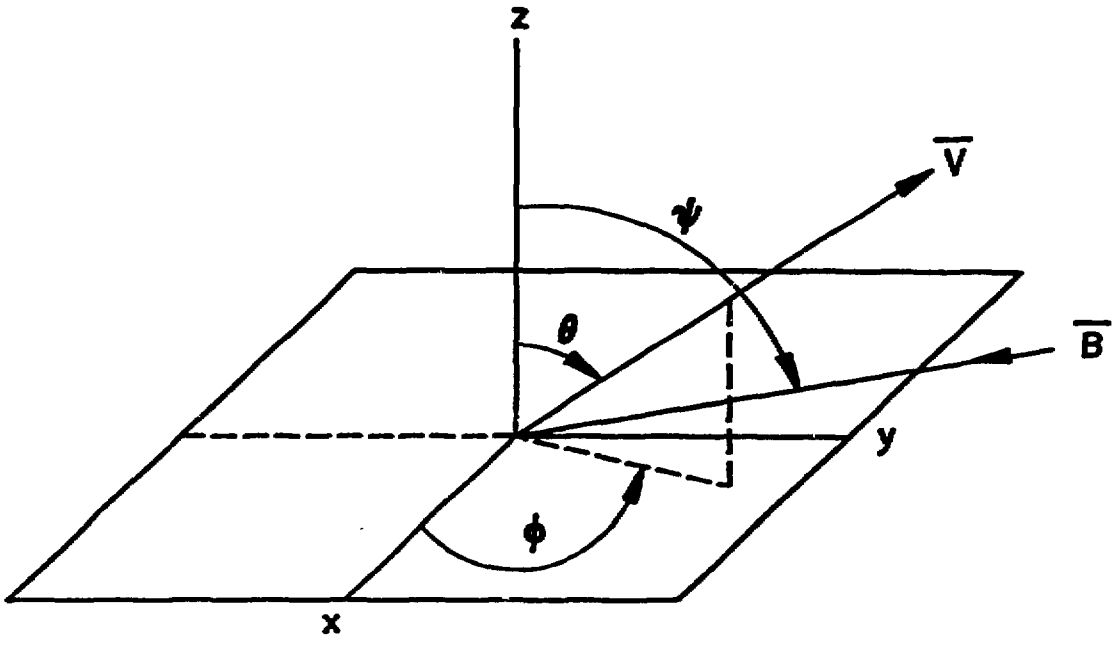

Figure 1. Model geometry.

collision cascade model [7], slightly modified to account for a maximum sputtered energy:

$$f_1(E) = \begin{cases} \dfrac{C\, E_B E}{(E + E_B)^3}, & E \le E_{max} \\ 0, & E > E_{max} \end{cases} \qquad (2)$$

where E_B is the surface binding energy (11.4 eV-tungsten, 7.4 eV-carbon) and C is a normalization constant. The maximum sputtered energy is taken as $E_{max} = 3\,|e\phi_o|$ where e is the proton charge and ϕ_o is the sheath potential. (The results were found to be only weakly dependent on E_{max}.) The angular distributions used for physically sputtered atoms are as follows:

$$f_2(\theta) = \cos\theta$$

$$f_3(\phi) = \frac{1}{2\pi} \qquad (3)$$

These are appropriate for normal incidence particle sputtering. (The effects of some variations in angular distribution were found to be small, in the regime studied.)

A sputtered atom has a speed given by:

$$\frac{1}{2} M_a V_o^2 = E \tag{4}$$

for impurity mass M_a. The probability of ionization is determined from the locally-varying mean free path:

$$\lambda = \frac{V_o}{N_e \langle \sigma V \rangle_{i,o}} \tag{5}$$

where N_e is the electron density and $\langle \sigma V \rangle_{i,o}$ is the rate coefficient for electron impact ionization of the sputtered atom. In the code the particles are launched, and the point of ionization determined, by standard Monte Carlo methods.

2.2 Ion Transport

Once ionized, the particle velocity is given by:

$$\frac{d\bar{V}}{dt} = \frac{q}{M_a} (\bar{E} + \bar{V} \times \bar{B}) + \frac{\partial \bar{V}}{\partial t} \Big|_{\text{collisions}} \tag{6}$$

for ion charge $q = Ke$, where $K = K(t)$ is the charge state. For the (tokamak edge) plasmas considered, the impurity ion-plasma collision time, τ_c, is much longer than an impurity ion gyroperiod, τ_g. Eq. 6 is therefore solved as follows. For short time increments, $\Delta t_o < \tau_g$ the Lorentz force motion only is computed, via a second order implicit method. After multiple time steps, N, such that $\tau_g < N\Delta t_o < \tau_c$, the effect of collisions is computed by perturbing the velocity. This is done via the standard Fokker-Planck equations:

$$V_\parallel = V_{\parallel_o} + \langle \Delta V_\parallel \rangle \Delta t_c \pm \sqrt{\langle \Delta V_\parallel^2 \rangle \Delta t_c} \tag{7}$$

$$V_\perp = \pm \sqrt{\langle \Delta V_\perp^2 \rangle \Delta t_c}$$

where $V_\parallel$ denotes the speed in the direction initially parallel to $\bar{V}$, i.e., prior to the collision, $V_\perp$ is the speed in the initially perpendicular direction, $\Delta t_c = N\Delta t_o$, and $\langle \Delta V_\parallel \rangle$, $\langle \Delta V_\parallel^2 \rangle$, and $\langle \Delta V_\perp^2 \rangle$ are the parallel friction, parallel velocity diffusion coefficient, and perpendicular velocity diffusion coefficient, respectively. The choice of plus or minus signs in (7) are chosen randomly, per the Monte Carlo treatment. Except as otherwise noted, the standard Braginski-Spitzer coefficients [8,9] appropriate to electron, DT ion-impurity ion collisions are used.

The ion charge state is computed based on the following probabilities. During a time step Δt_o, the probability of an ion changing charge is given by:

$$P_1 = 1 - \exp\left(-\Delta t_o / \tau_K\right) \tag{8}$$

where

$$\tau_K = \frac{1}{N_e\left[\langle \sigma V \rangle_{i,K} + \langle \sigma V \rangle_{r,K}\right]} , \tag{9}$$

$\langle \sigma V \rangle_{i,K}$ is the rate coefficient for ionization from the K to K+1 state, and $\langle \sigma V \rangle_{r,K}$ is the rate coefficient for recombination from the K to K-1 state. If a change in state occurs, the probability that the change is due to ionization is given as:

$$P_2 = \frac{\langle \sigma V \rangle_{i,K}}{\langle \sigma V \rangle_{i,K} + \langle \sigma V \rangle_{r,K}} \tag{10}$$

Ionization rate coefficients from Ref. [2] are used for tungsten (assumed to be limited to $K \leq 11$) and from Ref. [10] for carbon. Recombination coefficients from the ADPAK Code [11] are used for both materials.

2.3 Sheath Region

Analysis of the oblique incidence sheath (Refs. [3-6]) has shown that the sheath divides into a debye sheath region of the order of several debye lengths and a "magnetic sheath" region of the order of the D-T ion gyroradius, R_{DT}. The sheath potential, ϕ_o, is approximately independent of incidence an-

gle ψ, but the potential difference in each region varies with ψ. As $\psi \to 90°$ the magnetic sheath becomes dominant. Based generally on these results, the potential is modeled as having the following dual structure:

$$\phi(z) = \phi_1 \exp(-Z/2\lambda_D) + \phi_2 \left(-Z/R_{DT}\right) \tag{11}$$

where $\phi_1 + \phi_2 = \phi_0$, and λ_D is the debye length at the start of the sheath.

A parameter, γ_D, defined as the fraction of sheath potential occurring in the debye region, is used to specify ϕ_1 and ϕ_2:

$$\gamma_D = 1 - \frac{\phi(6\ \lambda_D)}{\phi_0} \tag{12}$$

where, as indicated, the width of the debye sheath is taken as six debye lengths, i.e., 3 e-folding distances. Except as otherwise noted, the electric field and electron density are given by:

$$E_x = E_y = 0$$

$$E_z = -\frac{d\phi}{dz} \tag{13}$$

$$N_e = N_{e_o} \exp\left(e\phi/kT_e\right)$$

where N_{e_o} is the electron density far from the sheath, and T_e is the electron temperature. A constant electron temperature and $T_i = T_e$ is assumed. The plasma flow velocity, prior to the sheath is given by the sound speed.

3. RESULTS

3.1 WBC Code

In the code 1000 particles were launched for each calculation. This number of particles was found to give an acceptably small statistical error, typically within ~ ±5%. A particle history terminates upon reaching the surface, i.e., z=0. Redeposited particle parameters such as the transit time, τ_R, energy U, and incident angles are then computed. Self-sputtering

coefficients for redeposited particles are computed for tungsten, using the DSPUT code [12] with inputs of energy and elevation angle.

3.2 Reference Case

For computational purposes, a reference plasma was defined, with typical tokamak divertor parameters B=5T, ψ=87°, $e\phi$=-3kT_e, and γ_D=0.25. The latter value is typical of results obtained [4-6,13] for highly oblique field angles. The above values are used throughout except where otherwise noted.

Table 1 compares results for tungsten and physically sputtered carbon for a medium edge temperature case of T_e = 75 eV, N_{e_o} = 10^{20} m^{-3}, and Figs. 2-3 show the charge state and elevation angle distribution of redeposited tungsten for this case. A key difference between tungsten and carbon sputtering is the smaller neutral ionization distances for tungsten. This is simply due to the much higher tungsten mass and somewhat higher (~ 2x) ionization cross section. Sputtered tungsten tends to be ionized within the magnetic sheath region (3 R_{DT} = .84 mm for T_e = 75 eV) while most carbon is ionized well outside of the sheath. Compared to previous estimates [2] sputtered tungsten returns to the surface faster due to acceleration by the sheath field. Carbon ions depend more on collisions to return to the surface.

Table 1
Redeposited ion parameters for tungsten and physically sputtered carbon. For plasma parameters T_e = 75 eV, N_e = 10^{20} m^{-3}, ψ = 87°, f_D = 0.25, $e\phi$ = -3 kT_e.

Parameter*		Value Tungsten	Carbon
Neutral ionization distance (perpendicular to surface)	$\bar{Z}_o$	.40 mm	1.7 mm
Transit time	$\bar{\tau}_R$	.60 μs	2.2 μs
	$\tau_{R_{SD}}$	1.6 μs	3.2 μs
Elev. angle	$\bar{\theta}$	18°	41°
Azimuth angle	$\bar{\phi}$	141°	106°
Charge state	$\bar{K}$	2.6	2.0
	K_{SD}	2.5	1.1
Energy	$\bar{U}$	553 eV	468 eV
	U_{SD}	691 eV	333 eV

* Bar denotes average value, SD denotes standard deviation.

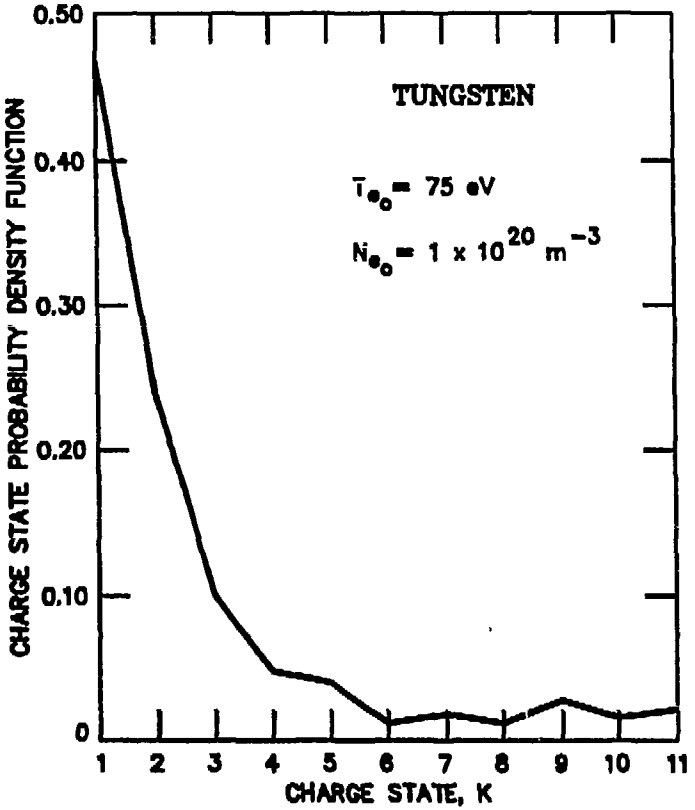

Figure 2. Charge state distribution of redeposited tungsten.

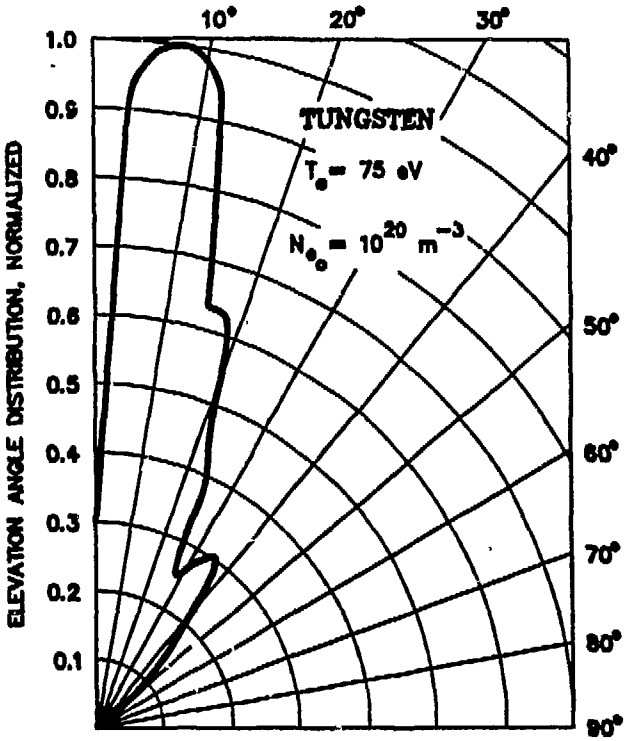

Figure 3. Elevation angle distribution of redeposited tungsten.

Figures 4-6 show the average values of charge state, energy, and self-sputtering coefficient of redeposited tungsten for a range of plasma conditions. These conditions span much of the range expected near a divertor plate or a limiter, for low to medium plasma edge temperatures. As shown, the average charge state is relatively insensitive to temperature but is sensitive to density. The former is due, in part, to the weak variation in ionization rate coefficients with temperature. The average energy increases with T_e, basically scaling with sheath potential. The average self-sputtering coefficient scales in a similar manner as the average energy. This is expected for near-normal incidence of tungsten, for the energy domain in question. There is a significant region of the T_e, N_{e_o} range where the self-sputtering coefficient is less than unity, a necessary condition for a surface material to avoid a runaway self-sputtering cascade.

Figure 7 shows the variation in $\bar{K}$ with T_e and N_{e_o} for carbon. The trend is similar to that for tungsten. In addition it is found that no carbon ions are present in charge states K = 5 or 6. This follows from the fact that the redeposition transit times are much less than the characteristic time for ionization of the K = 4 state, for example for $N_{e_o} = 10^{20}$ m^{-3}, T_e = 75 eV:

$$\frac{\bar{\tau}_R}{\tau_{i,4}} = 2 \times 10^{-4}$$

where

$$\tau_{i,4} = \frac{1}{N_{e_o} \langle \sigma V \rangle_{i,4}} \quad .$$

For this reason, $\bar{K}$ is considerably less than the coronal equilibrium value, which for example, is about 4 at 75 eV [14].

Figure 8 shows the variation in several carbon transport parameters with density, for T_e = 75 eV. The self-sputtering coefficient was not computed for carbon but is known to depend strongly on incidence elevation angle. The latter becomes more oblique at lower densities, as shown. The transit time increases rapidly as $N_{e_o} \to 0$ for two reasons: (1) Carbon atoms are ionized

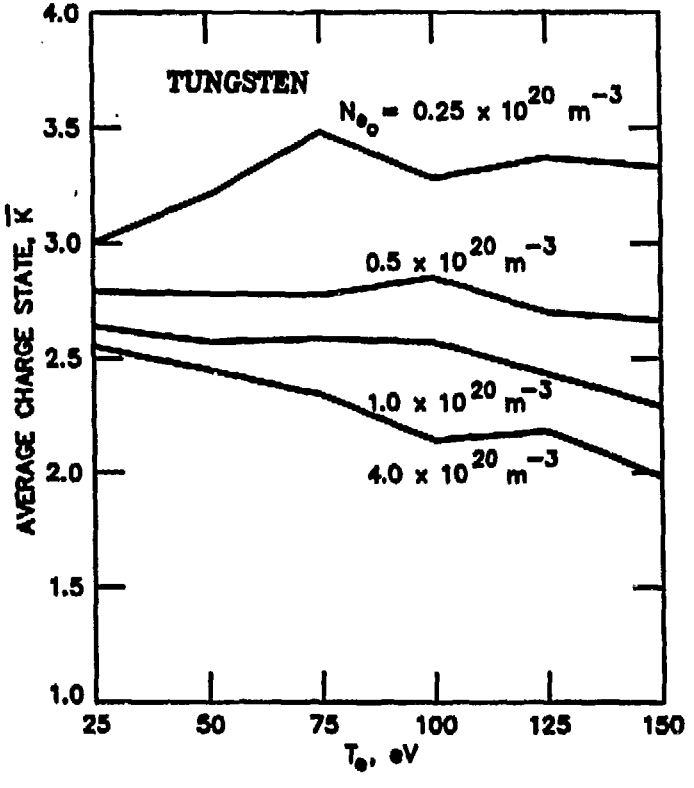

Figure 4. Average charge state of redeposited tungsten as a function of plasma temperature and density.

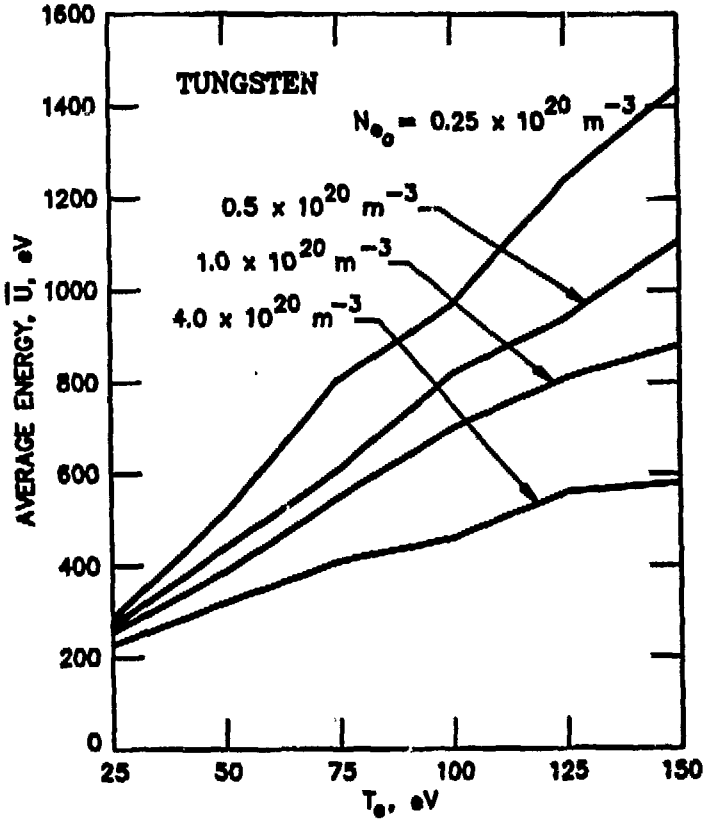

Figure 5. Average energy of redeposited tungsten as a function of plasma temperature and density.

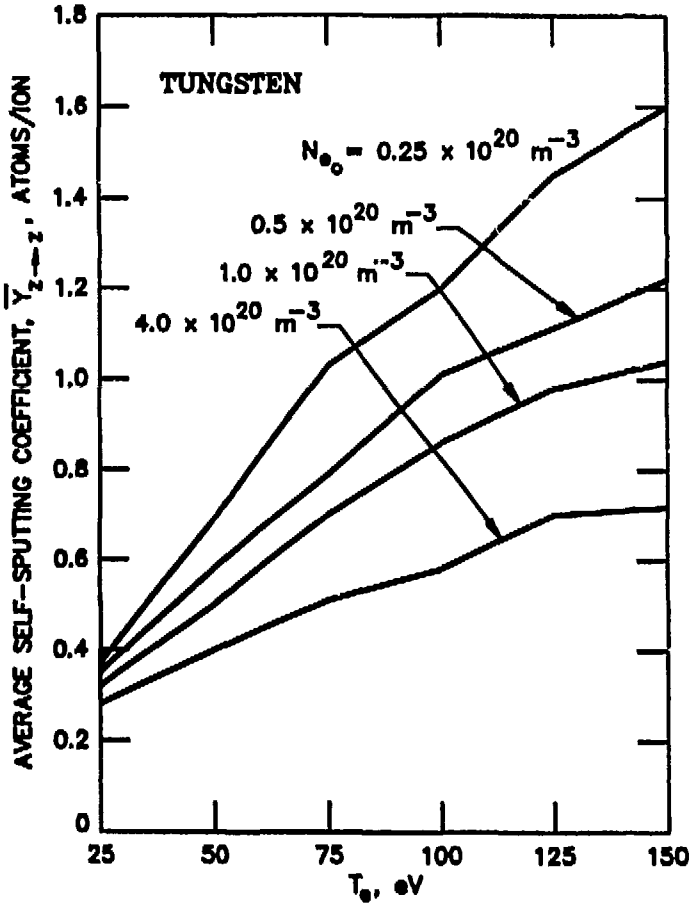

Figure 6. Average self-sputtering coefficient of redeposited tungsten as a function of plasma temperature and density.

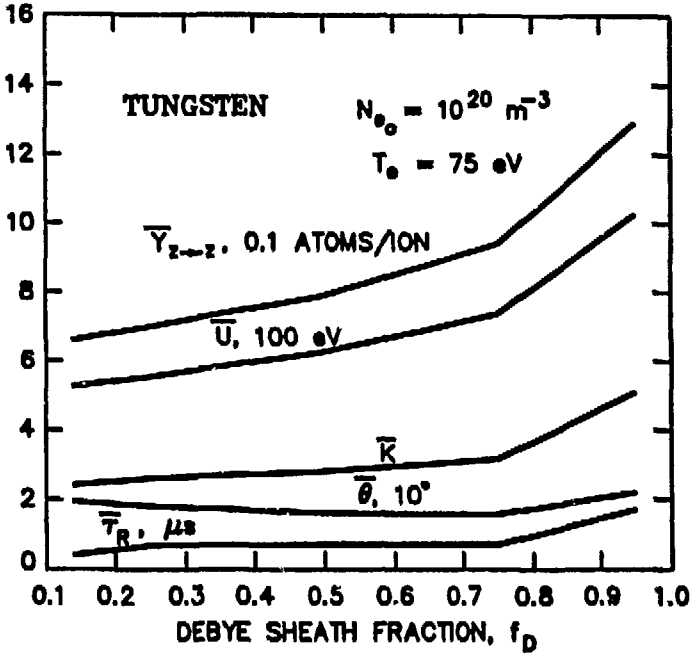

Figure 7. Sensitivity of redeposited tungsten parameters to the sheath parameter f_D.

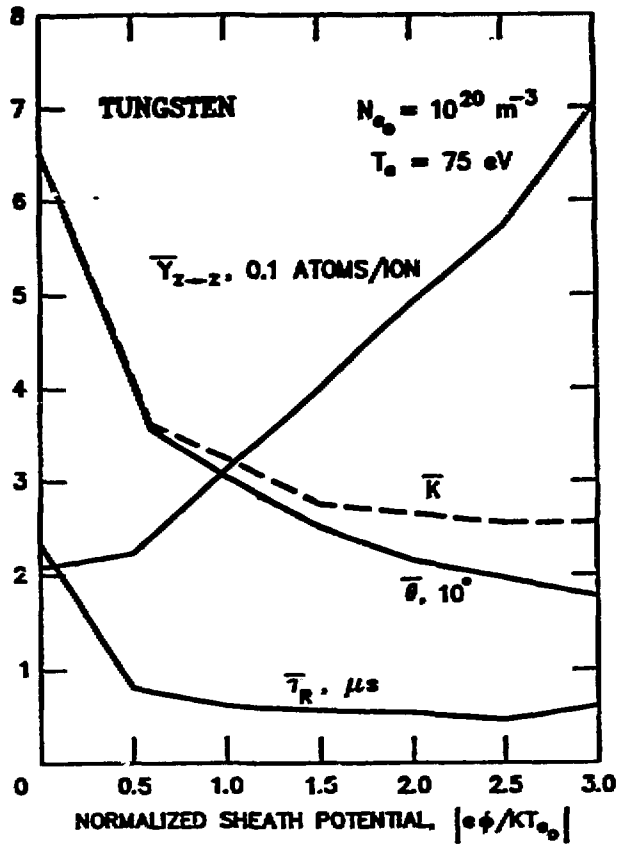

Figure 8.
Sensitivity of redeposited tungsten parameters to the sheath potential.

farther from the surface, and (2) The collision frequency, scaling as $\tau_c \sim N_{e_o}^{-1}$, decreases. It should be noted that at lower N_{e_o}, the transport region extends sufficiently far from the surface that the spatial variations in plasma parameters would need to be taken into account, to adequately assess the particle transport. In particular, sputtered particles entering regions of stagnant plasma flow would tend not to be redeposited locally. However, the results shown here should show the basic trends for carbon at low N_{e_o}.

3.3 Effect of Sheath Parameters

The importance of several sheath parameters to the sputtered particle transport was examined for tungsten. Figure 9 shows the effect of variations in the debye sheath fraction. The lower and upper limits on f_D correspond to $\phi_2 = 0$ (magnetic sheath only) and $\phi_1 = 0$ (debye sheath only) respectively. The transport is relatively insensitive to f_D at lower values but quite

sensitive near the debye limit. In this case most sputtered atoms are ionized outside of the sheath region and so depend primarily on impurity-plasma collisions to return them to the surface. This is a slower process than electric field acceleration which enables the tungsten ions to reach significantly higher charge states.

Figure 10 shows the sensitivity to sheath potential. As expected, this has a substantial effect on the results particularly the self-sputtering coefficient. The sensitivity to the magnetic field angle was also examined. No statistically significant differences were observed for tungsten, for $80° \leq \psi \leq 89°$, for $N_{e_o} = 10^{20}$ m^{-3}, $T_e = 75$ eV.

3.4 Other Cases

Transport of low energy sputtered carbon was examined. This can arise from radiation enhanced sublimation (RES) which results in thermally emitted carbon atoms [15]. RES carbon transport was examined for $T_e = 150$ eV, a temperature where RES is thought to be a serious limitation on a carbon divertor surface operating temperature [16]. In the code, RES carbon atoms were simulated by launching with velocities chosen from a normal distribution in each orthogonal component, corresponding to a carbon surface temperature of 1000 C. Average values of charge state and normalized energy were found as follows: $\bar{Z} = 1.2$, 1.1, $|\bar{U}/e\phi| = .96$, .73 for plasma densities of $N_{e_o} = .1 \times 10^{20}$ m^{-3}, and $.25 \times 10^{20}$ m^{-3}, respectively.

The effects of viscosity, thermal forces, and a radial electric field were examined. These phenomena may arise in a divertor plasma where high temperature and density gradients are present because of high local recycling. Viscosity and thermal forces were examined separately by including appropriate collision terms in Eq. (7). These collision terms, for trace impurity ions in a D-T plasma, are taken from Ref. [17]. Viscosity effects were examined using values of plasma flow velocity gradients parallel and perpendicular to the magnetic field of 10^8 s^{-1} and 3×10^4 s^{-1} respectively. Thermal forces were computed using parallel temperature gradients of $T_e' = T_i' = -30$ eV/m. These values are equal to or greater than those computed by a fluid code for a drift-dependent, high recycling divertor [18]. Code runs were made for both tungsten and carbon, for $T_e = 75$ eV, $N_{e_o} = 10^{20}$ m^{-3}.

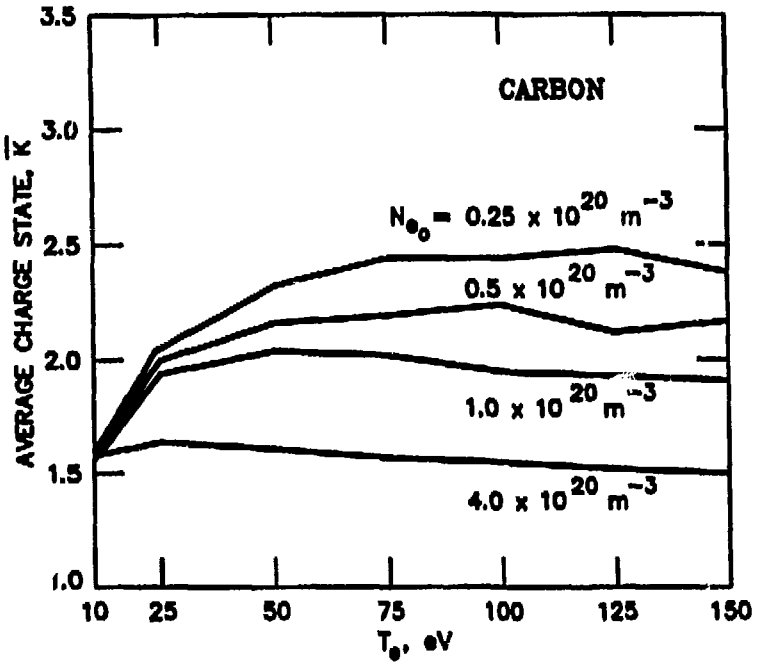

Figure 9. Average charge state of redeposited carbon as a function of plasma temperature and density.

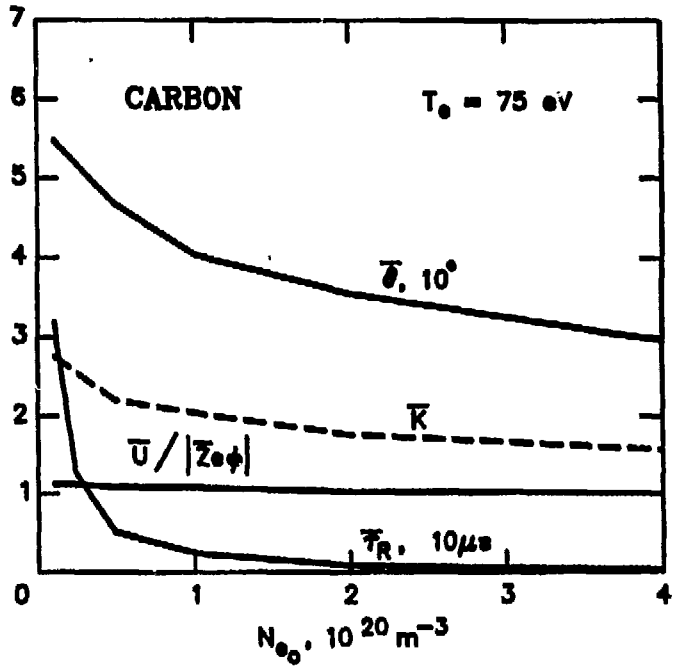

Figure 10. Redeposited carbon parameters as a function of plasma density.

The results for both the viscosity and thermal force calculations showed no statistically significant differences from the reference case. Evidently, the transit times for impurity transport for the above plasma conditions are too short for viscosity and thermal forces to have an effect. This of course, need not be true for impurities present in the scrapeoff layer farther from the surface.

It is not known what radial electric field, if any, would be present at and near the plasma-surface boundary. The effect of a hypothetical radial field of E_x = -5000 V/m was examined, for the above plasma parameters. This field results in a substantial decrease in average transit times (~ factor of two) and smaller but significant decreases in redeposited charge states and energy; results for carbon are: $\bar{K}$ = 1.7, $\bar{U}$ = 370 eV, and for tungsten: $\bar{K}$ = 2.3, $\bar{U}$ = 472 eV, $\bar{Y}_{z-z}$ =.62.

4. CONCLUSIONS

Sputtered particle transport has been analyzed for representative tokamak edge conditions. The results should provide guidance for erosion and plasma edge parameter analysis. Sputtered tungsten atoms tend to be ionized within the oblique magnetic field sheath, which has a marked influence on their subsequent transport. Redeposited tungsten ions tend to impact at near normal incidence, with average charge states varying from 2-3.5. A tungsten divertor surface may be feasible, from the self-sputtering standpoint, for plasma temperatures as high as about 100 eV. Physically sputtered carbon tends to be redeposited with average charge states varying from 1.5-2.5. For both impurity species the transit time from sputtering to redeposition is generally smaller than the impurity plasma collision time, over most of the edge plasma regime studied. Radiation enhanced sublimated carbon tends to be only singly ionized but still acquires a significant energy in sheath acceleration.

REFERENCES

1. J.N. Brooks, Nuc. Tech./Fusion 4 (1983) 33.
2. C.D. Boley, J.N. Brooks, and Y.K. Kim, Argonne National Laboratory Report ANL/FPP/TM-171 (1983).
3. V. Daybelge and B. Bein, Phys. Fluids 24 (1981) 1190.

4. R. Chodura, Phys. Fluids 25 (1982) 1628.

5. R. Chodura, in Physics of Plasma - Wall Interactions in Controlled Fusion, D.E. Post and R. Behrish, editors, Plenum Publishing (1986).

6. A.B. Dewald, A.W. Bailey, and J.N. Brooks, Phys. Fluids 30 (1987) 267.

7. M. Thompson, Philos. Mag., 18 (1968) 377.

8. S.I. Braginskii, in Reviews of Plasma Physics, Vol. 1, M.A. Leontovich, ed., Consultants Bureau (1965).

9. L. Spitzer, Jr., Physics of Fully Ionized Gases, 2nd Edition, Wiley (1962).

10. K.L. Bell et al., Culham Laboratory Report CLM-R216 (1982).

11. R. Hulse, personal communication (1985).

12. D.L. Smith et al., Proc. 9th Symp. on Engineering Problems of Fusion Research, IEEE publication 81CH1715-2 (1981) 719.

13. R. Chodura, personal communication (1989).

14. D.E. Post et al., Atomic Data and Nuclear Tables, Vol. 20, Academic Press, New York, NY (1978) 397.

15. J. Roth, J. Bohdansky, and K.L. Wilson, J. Nuc. Mat. 11&12 (1982) 775.

16. J.N. Brooks, "Temperature Limit of a Graphite Divertor Surface Due to Self-Sputtering and Radiation Enhanced Sublimation," J. Nuc. Mat. (to be published).

17. W.K. Terry, Argonne National Laboratory Report ANL/FPP/TM-215 (1988).

18. M. Petravic, G. Kuo-Petravic, and T. Arnzt, Contributions to Plasma Physics, 28 (1988) 379.